Membrane tension regulates motility by controlling lamellipodium organization

Ellen L. Batchelder[a,b,c], Gunther Hollopeter[d,e,1], Clément Campillo[a,b,c], Xavier Mezanges[a,b,c,f], Erik M. Jorgensen[d,e], Pierre Nassoy[a,b,c], Pierre Sens[g], and Julie Plastino[a,b,c,2]

[a]Institut Curie, Centre de Recherche, Paris, F-75248 France; [b]Centre National de la Recherche Scientifique, Unité Mixte de Recherche 168, Paris, F-75248 France; [c]Université Pierre et Marie Curie, Paris F-75248, France; [d]Department of Biology and [e]Howard Hughes Medical Institute, University of Utah, Salt Lake City, UT 84112-0840; [f]Université Paris Diderot, Sorbonne Paris Cité, Paris F-75248, France; and [g]Ecole Supérieure de Physique et Chimie Industrielles, Centre National de la Recherche Scientifique, Unité Mixte de Recherche 7083, Paris 75231, France

Edited by Alexander Mogilner, University of California, Davis, CA, and accepted by the Editorial Board May 27, 2011 (received for review July 19, 2010)

Many cell movements proceed via a crawling mechanism, where polymerization of the cytoskeletal protein actin pushes out the leading edge membrane. In this model, membrane tension has been seen as an impediment to filament growth and cell motility. Here we use a simple model of cell motility, the *Caenorhabditis elegans* sperm cell, to test how membrane tension affects movement and cytoskeleton dynamics. To enable these analyses, we create transgenic worm strains carrying sperm with a fluorescently labeled cytoskeleton. Via osmotic shock and deoxycholate treatments, we relax or tense the cell membrane and quantify apparent membrane tension changes by the membrane tether technique. Surprisingly, we find that membrane tension reduction is correlated with a decrease in cell displacement speed, whereas an increase in membrane tension enhances motility. We further demonstrate that apparent polymerization rates follow the same trends. We observe that membrane tension reduction leads to an unorganized, rough lamellipodium, composed of short filaments angled away from the direction of movement. On the other hand, an increase in tension reduces lateral membrane protrusions in the lamellipodium, and filaments are longer and more oriented toward the direction of movement. Overall we propose that membrane tension optimizes motility by streamlining polymerization in the direction of movement, thus adding a layer of complexity to our current understanding of how membrane tension enters into the motility equation.

major sperm protein | retrograde flow | Mos1

In crawling cells, motility is mainly driven by actin polymerization, which forms filaments beneath the leading edge cell membrane to make protrusions (1). In this scenario, polymerization is inhibited by the presence of the cell membrane, and membrane tension is thus commonly seen as an impediment to cell motility (2). Experiments show that lamellipodial extension rate is indeed inversely correlated with membrane tension (3), but steady-state, whole cell translocation has not been studied. Here we use a simplified system of crawling cell motility, the *Caenorhabditis elegans* sperm cell, in order to address the question of how membrane tension affects whole cell translocation. The sperm cell contains only cytoskeleton, mitochondria, and nuclear material and is incapable of de novo protein synthesis or classical exo- and endocytosis, thus representing a useful model for exploring the interplay between membrane tension and cell motility. The sperm cell translocates by adhering to the substrate and emitting a dynamic lamellipodia, in a manner that is morphologically similar to actomyosin containing motile cells, despite the fact that the movement of sperm cells is powered by the dynamics of the major sperm protein (MSP) cytoskeleton in the absence of actin and known molecular motors (4, 5).

The production of fluorescently labeled actin in living cells was a watershed in the understanding of how actin structures assemble, flow, and disassemble to produce cell motility. However, due to efficient gene silencing mechanisms in the sperm cell and a lack of specific promoters for sperm cell expression, sperm cells carrying fluorescently labeled MSP have not been available. Here, we succeed in creating transgenic worm strains that produce sperm carrying fluorescently labeled MSP, active for polymerization. Using these sperm cells, we measure cell translocation and the dynamics of the MSP cytoskeleton under different conditions of membrane tension, as quantified by an optical tweezer/membrane tether approach (6). Unexpectedly we find that increases in tension actually speed up motility. We propose that membrane tension is a master regulator of lamellipodial directionality and that the benefits of having a tense membrane within some range outweigh the negative effects on polymerization. It will be interesting to see if this paradigm is applicable to actin-containing cell types as well.

Results and Discussion

Production of Worm Strains Carrying Fluorescent Major Sperm Protein. We generated transgenic worm strains that produced MSP-142 labeled on the N terminus with tagRFP-T (7) specifically in sperm cells via either the *peel-1* promotor (8) or the *spe-11* promotor, using the Mos1-mediated single-copy insertion technique (9) (Fig. 1*A*). When extruded from male worms and activated by pronase digestion to form lamellipodia (10), strains carrying the *spe-11* promotor gave sperm cells with fluorescent lamellipodia that were mottled in appearance, whereas fluorescence was dim and diffuse in the cell body (Fig. 1*B*). Strains carrying the *peel-1* promotor gave enhanced fluorescence allowing for the visualization of MSP superstructures in the lamellipodium (Fig. 1*B* and Movie S1). Similar fiber complexes had previously been observed by electron microscopy in the sperm from the nematode *Ascaris* (4). In addition, in *peel-1* strains, MSP fluorescence was evident at the plasma membrane encasing the cell body.

Active sperm cells either adhered and crawled on the substrate or were stationary but maintained a dynamic lamellipodium. In the stationary case, inability to translocate was due to a total lack of adhesion under the lamellipodium, as evidenced by the fact that these cells were either completely afloat and drifting, or the lamellipodium waved around an immobile cell body. In both crawling and stationary cells, fluorescent features were observed to flow in the lamellipodium. The localization of fluorescence in the cell and its dynamic properties indicated that

Author contributions: E.L.B., G.H., C.C., E.M.J., P.N., P.S., and J.P. designed research; E.L.B., G.H., C.C., and J.P. performed research; E.L.B., G.H., C.C., X.M., and J.P. analyzed data; and P.S. and J.P. wrote the paper.

The authors declare no conflict of interest.

This article is a PNAS Direct Submission. A.M. is a guest editor invited by the Editorial Board.

[1]Present address: Stowers Institute for Medical Research, Kansas City, MO 64110.

[2]To whom correspondence should be addressed. E-mail: julie.plastino@curie.fr.

This article contains supporting information online at www.pnas.org/lookup/suppl/doi:10.1073/pnas.1010481108/-/DCSupplemental.

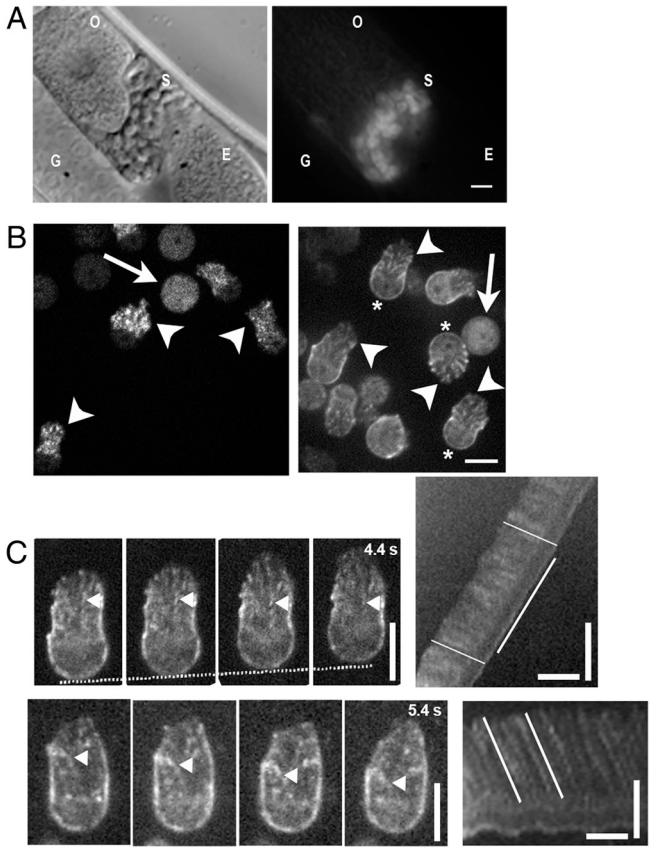

Fig. 1. *tagRFP-T::MSP is expressed exclusively in sperm cells and is competent for polymerization*. (*A*) A worm expressing MSP-142 N-terminally fused with tagRFP-T driven by the *spe-11* promoter. (*Left*) Transmitted light image; (*Right*) epifluorescence image. O, oocyte; G, gonad arm; S, spermatheca, and E, fertilized embryo. Fluorescence is seen only in the spermatheca, where sperm cells are stored. (*B*) A representative field of active and inactive sperm cells containing tagRFP-T::MSP driven by the *spe-11* promotor (*Left*) and the *peel-1* promotor (*Right*). In inactive round sperm cells, fluorescence is uniform (arrows), whereas in activated cells, fluorescence is concentrated in the lamellipodia and displays bright patches (arrowheads) or is visible as a cortex near the plasma membrane (asterisk, *peel-1* strains only). (*C*) Typical analysis of flows and movement of sperm cells by kymograph analysis. Kymographs were created from a line drawn on the long axis of the cell near the center. (*Top*) Still images of a crawling cell and associated kymograph. The position of the cell body is indicated by the white dotted line, and the time on the last panel is the total elapsed time. (*Bottom*) Still images of a stationary cell and associated kymograph. Arrowheads point to features undergoing retrograde flow toward the cell body and producing streaks in the kymographs. Examples of retrograde flow and movement lines are indicated on the kymographs. In *A* and *B* , bar = 5 μm. In *C*, vertical scale bar = 5 μm, and horizontal scale bar = 20 s.

tagRFP-T::MSP was competent for polymerization and integrated into filaments. N-terminal fusions with mCherry, EGFP, and citrine gave no or dim fluorescence, and none of the C-terminal fusions gave visible fluorescence, perhaps due to a protein stability problem as the C terminus participates in the subunit interface of the MSP dimer (11). Despite the difference in expression level, sperm cells from the *spe-11* and *peel-1* strains displayed identical motility speeds (Fig. S1), and in the following study, the two strains were used interchangeably.

To image cytoskeleton dynamics in moving sperm cells in vivo, we mated males carrying fluorescent sperm with spermless *fog-1* hermaphrodites. Mating activates male sperm to form a lamellipodium (10). We revealed the same two modes of movement in vivo as observed for extruded, pronase-activated cells, i.e., crawling cells and active, but stationary cells, indicating that this latter behavior was physiologically relevant (Movie S2). Because the behavior of extruded fluorescent sperm was qualitatively similar to that of in vivo sperm, and extruded sperm were easier to manipulate, we characterized MSP cytoskeletal dynamics and sperm cell movement using extruded, pronase-activated cells crawling on glass. By kymograph analysis, we analyzed cell displacement speed as well as retrograde flows during movement and stationary phases, as illustrated in Fig. 1*C* (Movie S3).

Effect of Membrane Tension on Movement. Using this experimental system, we probed the role of membrane tension in cell movement and cytoskeleton dynamics. Following published methods, we inflated cells by hypoosmotic shock thus tensing the membrane, or we relaxed the cell membrane either by hyperosmotic shock, which deflates cells, or via low concentrations of the detergent deoxycholate, known to decrease membrane tension without changing cell volume (3). In all cases, decreasing membrane tension universally led to a decrease in the speed of cell translocation (Fig. 2*A*). On the contrary, swelling the cells resulted in an increase in the speed of cell translocation. We verified that we were indeed affecting cell volume by measuring the spread area of crawling cells: Under hypoosmotic shock, cells were significantly larger than control cells or deoxycholate-treated cells, while hyperosmotically shocked cells were significantly smaller (Fig. 2*B*). In the model where membrane tension is seen as a barrier to cytoskeletal polymerization, one could expect that relaxed membrane conditions might result in comparatively longer cells, but this was not the case, as shown by the fact that the aspect ratio of the cells was identical under all conditions tested (Fig. 2*B*).

To confirm that we were really affecting membrane tension via our osmotic shock and deoxycholate treatments, we measured effective membrane tension via the membrane tether technique. In these experiments, the force needed to pull a thin membrane tube from the surface of a cell is measured using an optical tweezer setup (12), and this tether force f_t can be related to an effective membrane tension (or "cell tension") σ, which comprises the tension of the lipid bilayer, but also the attachment of the cytoskeleton to the membrane, through the relationship $\sigma = f_t^2/(8\pi^2\kappa)$, where $\kappa \approx 10^{-19}$ N.m is the bending rigidity of the tether membrane (13, 14). We observed that tether forces were significantly lower for cells under relaxed membrane conditions, mirroring the effects observed on cell speed (Fig. 2*C* and Movie S4). For hypoosmotic shock, tethers pulled after the 30–45 min time span it took to set up a tube-pulling experiment exhibited the same force as control cells. However, when we pulled tubes in isotonic medium and held them steady as we flowed in water to dilute the media, we observed a reproducible spike in tether force, which was never observed in control tubes (Fig. 2*D*). These results suggest that cells confronted with hypoosmotic shock relaxed their membrane tension over long times, perhaps due to passive fusion of membranous organelles with the plasma membrane. Speed measurements were always taken within 20 min after the application of hypoosmotic shock, so presumably before cell adjustment could set in. The tether force relaxation observed after the spike in Fig. 2*D* is of unknown origin, but does not seem to represent cell adjustment as it is also observed in control cells (Fig. 2*D*, blue curve) and has been observed in other cell types in the absence of osmotic shock (15). Under isotonic conditions, similar tether forces were obtained when tubes were pulled from the cell body or from the lamellipodium of activated sperm cells, despite the fact that the MSP cytoskeleton by fluorescence microscopy was of different densities and organizations in these different regions. This argued in favor of tether forces being a reflection of real membrane tension, although we cannot rule out a cytoskeleton contribution. Comparing strong hypertonic and isotonic conditions, there was a fivefold variation of the apparent membrane tension (from $\sigma \approx$ 0.03 pN/nm in strong hypertonic medium to $\sigma \approx 0.15$ pN/nm in

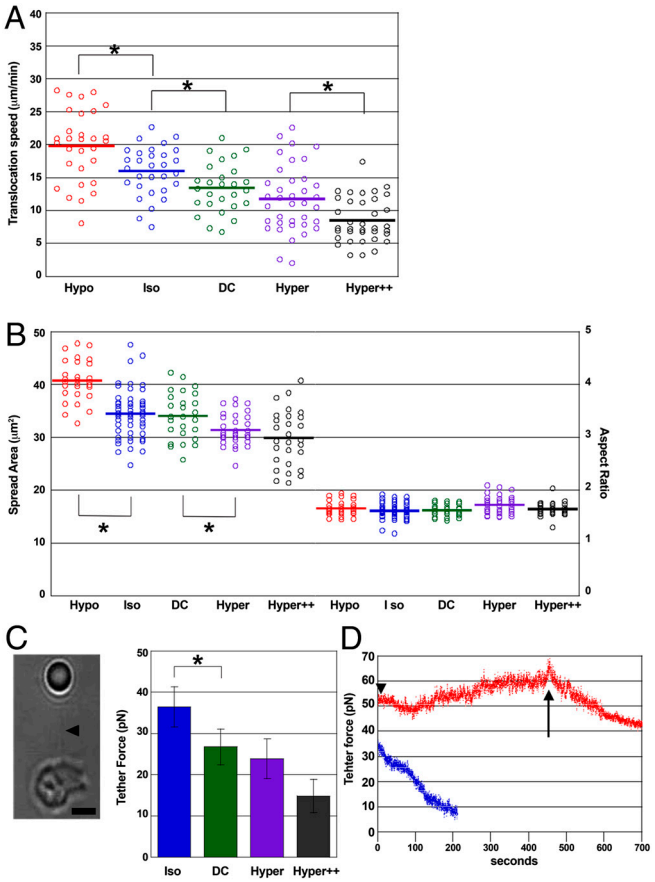

Fig. 2. *Effect of membrane tension on sperm cell motility.* (*A*) Dot plots of the speed of whole cell translocation. Red: hypotonic medium (130 mOsm); blue: isotonic media (175 mOsm); green: 150 μm deoxycholate (DC); purple: hypertonic media (275 mOsm); black: strong hypertonic media (350 mOsm). Significant differences are marked with asterisks. (*B*) Dot plots of the spread area of crawling cells and their aspect ratio (lamellipodium long axis divided by cell body width) under different treatments with labels and color coding as in *A*. Significant differences are marked with asterisks. (*C*) The relation of tether force (+/− SEM) to cell treatment. Legend is as for *A*. Seven to 18 cells were measured per condition, and tether forces were recorded as soon as the force stabilized (10–30 s), before tube relaxation could set in. The difference between Iso and DC/Hyper/Hyper++ is significant (marked with an asterisk for DC only). (*Left*) A tube (arrowhead) extending between the bead (*Top*) and the lamellipodia of a pronase-activated sperm cell (*Bottom*). The sperm cell is out of focus. (*D*) Tube under flow experiment to evaluate effect of hypotonic treatment on short time scales. A tube was pulled at time zero and 10 s later, water began to be injected (red curve, arrowhead) or not (blue curve). Evolution of the tether force was recorded over time and reproducibly showed a spike after water injection (red curve, arrow) before relaxing, whereas tubes of control cells just relaxed (blue curve). In *C*, bar = 2 μm.

isotonic medium, calculated with $\kappa \approx 10^{-19}$ N.m). We concluded that, opposite to established models for crawling cell movement, increased membrane tension enhanced cell movement, whereas decreased membrane tension inhibited sperm cell motility.

A decrease in movement with hypertonic treatment has been observed for cells that employ a blebbing mechanism of motility, such as the amoeba *Dictyostelium* and Walker carcinosarcoma cells (16, 17). Hypertonic medium reduces internal pressure and thus interferes with bleb formation and rapid movement. Sperm cells showed no apparent blebbing behavior by transmitted light microscopy, and no signature cytoskeleton arcs or membrane bulges devoid of MSP fibers were evident when the cell membrane was marked with a fluorescent dye and dual imaging of membrane and MSP cytoskeleton was performed (Movie S5).

Membrane Tension Controls Cytoskeleton Dynamics. Cell crawling is a complex process involving polymerization, cell-substrate adhesion, and retraction of the back of the cell during movement. Changes in membrane tension could affect any one of these parameters and reduce or augment displacement speed. We therefore calculated apparent polymerization rates under different membrane tension conditions by summing up forward movement and whatever was "lost" to retrograde flow (18). Retrograde flow in translocating sperm cells was measured as described in Fig. 1*C* and was found to be of low magnitude but nonzero, and independent of membrane tension conditions (Fig. 3*A*). However when we summed the absolute values of retrograde flow with the respective translocation speed, we observed that tension relaxation produced a reduction in apparent polymerization rates, whereas tension increase enhanced measured polymerization rates (Fig. 3*B*, *Left*).

This observation was further confirmed by measuring the retrograde flows of stationary cells under the different membrane tension conditions. The stationary, active cell is a particularity of nematode sperm; in the absence of adhesion, actin-containing cells lose polarity and round up. Although its role in nematode reproduction is unclear, the stationary sperm cell provides a tool for evaluating pure cytoskeleton turnover without adhesion and confirmed the downward trend in apparent polymerization speed with membrane relaxation (Fig. 3*B*, *Right*). Although rare events, single cells sometimes switched between crawling and stationary regimes, and when an algorithm was used to align the cell bodies of transitioning cells, all the slopes on the kymograph were the same, whether the cell was crawling or stationary (Fig. 3*C*). (For the aligned kymograph, the lines reported velocity with respect to the cell, instead of with respect to the substrate.) This meant that, from the cell perspective, there was no difference in cytoskeletal dynamics in the crawling versus the stationary case and supported the relevance of the stationary retrograde flow measurements as reflecting the apparent polymerization rate of the motile cell.

Membrane Tension Controls Lamellipodial Organization. From the point of view of a single growing filament, a floppy membrane is expected to provide the least hindrance to growth, so we sought an explanation for our results on a more global scale and hypothesized that lamellipodial organization could be controlled by membrane tension. To evaluate the 3D morphology of our cells, we labeled the membrane with a fluorescent dye and imaged active stationary cells via Z stacks (Fig. 4*A* and Movie S6). Cells under hypoosmotic shock had a smoother appearance than isotonic cells, whereas deoxycholate and hypertonic cells displayed numerous lateral protrusions. This was further confirmed in 3D when we reconstructed an XZ slice of the lamellipodium. The varying "roughness" of the lamellipodium is evident in the overlay of several typical contours (normalized for cell size) (Fig. 4*B*). We next quantified the roughness of the cell contour by comparing the contours to an ellipse and calculating the area of the deviations with a Matlab script. We found that membrane tension relaxation correlated with an increase in roughness of the lamellipodial membrane while it did not change the (much smaller) roughness of the cell body (Fig. 4*C* and Fig. S3). These observations strongly suggest that roughness is caused by underlying cytoskeleton in the lamellipodium exerting pushing forces against the membrane and deforming it.

To provide evidence for this hypothesis, we measured the distribution of fluorescent MSP fibers' orientation, θ, with respect to the direction of movement, which coincided with the long axis of the lamellipodium (defined as $\theta = 0°$) (Fig. 4 *D* and *E*). We observed that increasing membrane tension resulted in a narrower distribution of orientations (Fig. S4) and that fibers were on average more aligned with the lamellipodium long axis under high membrane tension conditions, with a mean fiber angle of approximately 30° in the case of hypoosmotic shock, and 55°

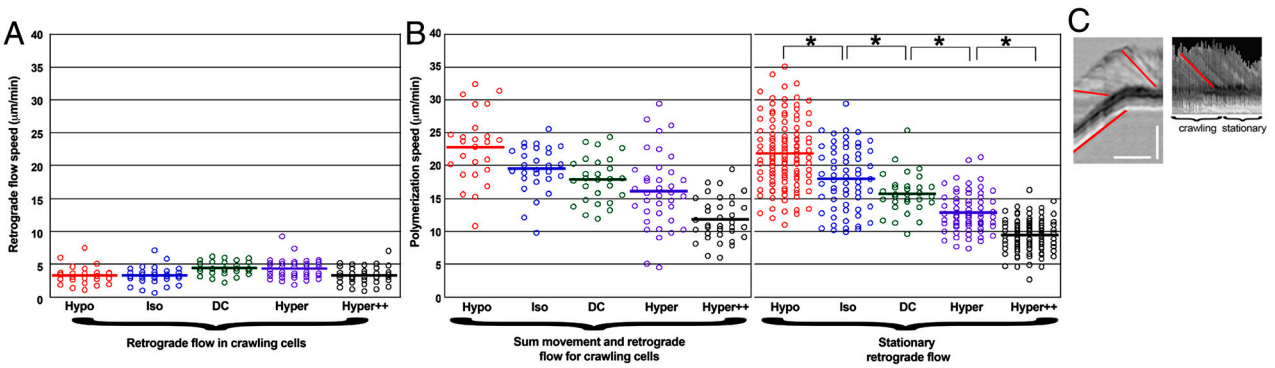

Fig. 3. *The effect of membrane tension on retrograde flow and apparent polymerization rates.* (*A*) Dot plots of speeds of retrograde flow (absolute values) during cell translocation. Red: hypotonic medium (130 mOsm); blue: isotonic media (175 mOsm); green: 150 μm DC; purple: hypertonic media (275 mOsm); black: strong hypertonic media (350 mOsm). (*B*) Polymerization speed under conditions as in *A*. (*Left*) Movement plus retrograde flow speeds (absolute values) for crawling cells. (*Right*) Retrograde flow speeds of stationary cells (absolute values). All differences in stationary retrograde flow values are significant (marked with an asterisk). The sum values give the same trend as the stationary retrograde flow values. (*C*) Transmitted light kymograph of a representative cell that transitions between translocating and stationary behaviors. [Features observable by transmitted light correspond to fluorescent MSP structures and show comparable dynamics (Fig. S2).] (*Left*) Normal kymograph, (*Right*) kymograph taken from the same cell but with the cell bodies aligned using a MatLab script. Example kymograph slopes drawn in red. Vertical scale bar = 5 μm, and horizontal scale bar = 15 s.

in the case of strong hyperosmotic shock (Fig. 4*E*). Polymerization contributes to retrograde flow in stationary cells and force production in motile cells only to the extent to which it is oriented along the long axis/direction of movement of the cell. Therefore fiber misalignment leads to an apparent polymerization velocity (the stationary retrograde velocity in nonmotile cells) smaller than the real polymerization velocity as expressed by the relation $v_{app} \approx v_p \langle \cos\theta \rangle$, where $\langle \cos\theta \rangle$ is the average fiber orientation (Fig. 4*F*). Indeed when we plot average apparent polymerization velocities from Fig. 3*B* versus $\langle \cos\theta \rangle$ under different membrane tension conditions, we obtain a linear correlation (Fig. 4*G*). The linear correlation provides evidence for the idea that membrane tension affects only the degree to which polymerization is streamlined in the productive direction and not the actual polymerization velocity. Additionally, we observed that enhanced alignment was concomitant with an increase in the average length of fibers (Fig. 4*H*).

It is conceivable that fiber length and alignment could derive from the cell size changes associated with osmotic shock; however, we saw the same trend with deoxycholate treatment, which does not affect cell size, pointing to a genuine effect of membrane tension. The exact mechanism of how tension reorganizes the lamellipodium would require a precise knowledge of fiber formation and the dynamics of fiber reorientation in a viscoelastic cytosol. Nevertheless, some insight on the streamlining effect of membrane tension on MSP fibers can be obtained by comparing the energy cost of membrane deformation around aligned and misaligned fibers (Fig. 4*F*). The diameter a of a fiber is likely to be larger than the diameter of an empty membrane tether, so the energy of the tubular membrane surrounding N independent fibers protruding a length L out of the cell is of order NE_1, where $E_1 \approx \sigma\pi aL$ is the membrane energy for a single fiber. If these fibers are parallel and close to one another, the energy becomes $E_N \approx \sigma\pi a_N L$, where $a_N \approx \sqrt{N}a$ is the diameter of the N-fiber bundle (estimated by simple volume conservation). There is thus a net energy gain $\Delta E_N \approx E_1(1 - 1/\sqrt{N})$ per fiber to join a N-fiber bundle. This simple argument (similar to the one proposed in ref. 19) shows the existence of membrane-mediated interactions that tend to coorient neighboring fibers, an effect that increases with membrane tension. The dependence of filament length on membrane tension could be due to the fact that the growing tips of aligned filaments remain longer in the polymerizing zone at the very tip of the lamellipodium. We verified the existence of a restricted polymerizing zone at the lamellipodium tip in our cells via photobleaching experiments (Fig. S5). MSP assembly occurred exclusively at the front of the cell and not along the sides or throughout the lamellipodium, and this was likewise the case under relaxed membrane tension conditions.

Concluding Remarks. In conclusion, production of a fluorescently labeled MSP cytoskeleton has allowed us to exploit the nematode sperm cell as a simple model of cell motility. We observe that MSP cytoskeleton displays many of the same dynamic principles as actin, such as localized leading edge cytoskeleton assembly, retrograde flow during movement, and displacement speed that is correlated with the speed of polymerization. We have used this system to evaluate how membrane tension affects cytoskeleton dynamics in a translocating cell. We conclude that membrane tension is necessary in the nematode sperm cell for optimal motility and that tension tends to orient filaments along the lamellipodium long axis, thus leading to a larger contribution of polymerization to movement or to stationary retrograde flow. There are indications in the literature that this strategy could also be operational in acto-myosin-containing cells. *Xenopus* epidermal cells show speed decreases upon hyperosmotic shock (20), whereas fish keratocytes are known to move better in 70% media (diluted with water) as opposed to undiluted media (21). If proven to be general to other cell types, our results will change how we think of membrane tension in the cell motility field.

Materials and Methods

Worm Strains, Culture and Sample Preparation. Standard procedures were used for culture of worms. All strains were grown and imaged at 20–23 °C. Using the Mos1-mediated single-copy insertion technique (9), two to seven independent homozygous single-copy insertion lines were generated with fluorescent tags fused to the N or C terminus of MSP-142, driven by the sperm specific promoter from *spe-11* and inserted at Mos 1 sites ttTi5605 on chromosome II or cxTi10882 on chromosome IV. Constructs carrying [*Pspe-11::tagRFP-T::msp-142::unc-54UTR*; (CB)*unc-119*(+)] II showed the highest levels of expression. Additionally, constructs of tagRFP-T fused to the N terminus of MSP-142 driven by the *peel-1* promoter with the *msp-142* UTR were created, and these lines displayed brighter fluorescence than the corresponding *spe-11* strains. The data in this study were generated from strains carrying N-terminally tagged MSP driven by the *spe-11* promoter (EG5160 and EG5164) or the *peel-1* promoter (EG5897). Male worms were produced either by heat shock or by crossing fluorescent strains with CB1489 [*him-8(e1489)*] IV.

Sperm cells were prepared as follows: Young adult male worms were isolated for 1 d, then picked into 5 μL of sperm media (50 mM Hepes, pH 7.0, 45 mM NaCl, 25 mM KCl, 1 mM $MgSO_4$, and 5 mM $CaCl_2$) with 16 mg/mL polyvinylprolidone (PVP) 40,000 molecular weight (Sigma) and 200 μg/mL of the activator Pronase (Sigma Protease P6911) on an untreated glass slide. An 18 × 18 mm coverslip was laid over the drop to crush worms and release sperm cells. The coverslip was sealed with a molten 1:1:1 mixture of Vaseline, Lanolin, and Parafilm (Valap), and samples were imaged immediately. The

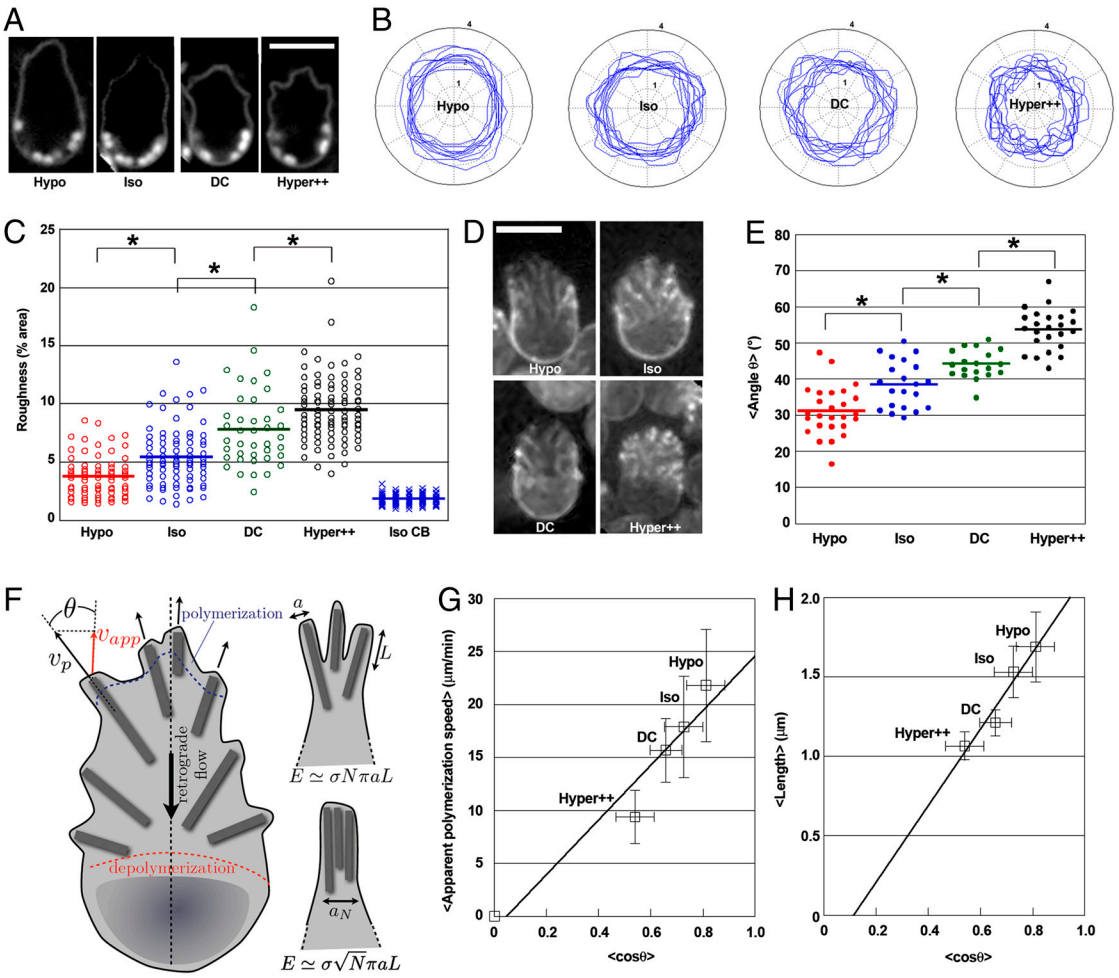

Fig. 4. *Tension controls lamellipodial organization in 3D*. (*A*) A confocal slice showing the plasma membrane labeling under different conditions of membrane tension. Hypo: hypotonic media (130 mOsm); Iso: isotonic media (175 mOsm); DC: 150 μm deoxycholate; Hyper++: strong hypertonic media (350 mOsm). (*B*) Overlay of 10 typical contours derived from XZ planes as described in *Materials and Methods* under conditions as in *A*. The inner concentric circle is at 1 μm and the outer circle is at 4 μm. (*C*) Roughness of lamellipodial contours under conditions as in *A*, with red: hypotonic medium; blue: isotonic media; green: 150 μm deoxycholate; black: strong hypertonic media. The roughness of the cell body under isotonic conditions is shown in blue -x- symbols. Roughness is represented as the percent of the total area involved in protrusions or invaginations that depart from the equivalent ellipse that matches the contour (see *Materials and Methods*). Significant differences are marked with asterisks. Cell body roughness under different tension conditions were not significantly different (Fig. S3) so only the isotonic data are shown. (*D*) MSP fiber visualization under different membrane tension conditions. Labels as in *A*. Images were denoised with the Safir program (see *Materials and Methods*). The lengths and angles of the fibers were measured for 20 such cells per condition to generate the data shown in *E*, *G*, and *H*. (*E*) Absolute values of fiber angles with respect to the long axis of the lamellipodium (defined as 0°) were averaged to give the average fiber angle (θ) per cell shown in dot-plot format. Color coding as in *C*. Asterisks mark significantly different populations. (*F*) Cartoon of a sperm cell with fibers as thick gray lines. Polymerization and depolymerization zones are delineated by blue and red dashed lines, respectively. The apparent polymerization speed (v_{app}, red arrow) corresponds to the projection (dotted line) of the polymerization flux (v_p, black arrow) along the cell axis and decreases with increasing filament misalignment (angle θ) according to the relation $\langle v_{app} \rangle = v_p \langle \cos\theta \rangle$. The energy cost of membrane deformation around finger-like protrusions is reduced when neighboring protrusions align with one another (see text). (*G*) Plot of average apparent polymerization speeds versus average $\cos\theta$ under four membrane tension conditions. All values +/– SD. The linear correlation is 0.97, with Hyper++ on the curve upon full extrapolation of the error bars in both the *x* and *y* directions. (*H*) Plot of average filament length versus average $\cos\theta$ under four membrane tension conditions. All values +/– SD. All length differences between the different conditions are significantly different. The linear correlation is 0.97. In *A* and *D*, bar = 5 μm.

membrane dye FM 1-43 (Molecular Probes) was added to the sperm media at a final concentration of 5 μg/mL. Deoxycholate (Sigma) was used at a concentration of 150 μM, and sucrose was added to a final concentration of 100 or 175 mM. The control conditions with sperm media, pronase, and PVP had an osmolarity of 175 mOsm. Osmolarities were measured on the Vapro 5520 vapor pressure osmometer (Wescor). For in vivo imaging of sperm cells, young adult CB4108 *fog-1* spermless females were mated with EG5897 males for 4–6 h, then incubated in paralytic solution [0.01% tetramisole (Sigma), 0.1% tricaine (Sigma)] for 30–60 min before being mounted on 3% agarose pads under a coverslip and sealed with Valap.

Image Collection and Analysis. Spinning disk confocal fluorescent images (paired with bright field) were acquired, and photobleaching experiments were performed at 23 °C on a Nikon Eclipse TE2000-E microscope equipped with an oil immersion objective 100× 1.40NA, a piezo stage (Nanoscan Prior), a Yokogawa CSU22 confocal head and a HQ2 CCD camera (Roper Scientific), 491- and 561-nm diode lasers for fluorescence excitation, and a head with 473- and 532-nm lasers for photobleaching (Roper Scientific laser launch) controlled by Metamorph software 7.5 (Molecular Devices) with the Live Replay function (Roper Scientific). Z stacks were acquired using the streaming function with 300 nm between planes (27 planes per stack). Whole worm phase contrast/fluorescence (Fig. 1*A*) was taken on an IX70 Olympus inverted microscope with an Olympus 100× 1.35NA phase-contrast objective (Olympus) equipped with a Mercury Arc lamp and recorded with a charge-coupled device camera (Roper Scientific) driven by MetaMorph software.

Image sequences were analyzed with the kymograph function of Metamorph 7.5 software. Differences between datasets were evaluated by an unpaired Student's *t* test, and a *p* value of 0.05 or less was considered significant. Spread areas and aspect ratios of crawling cells (natively activated, without addition of pronase) were measured by manually tracing cell out-

lines in fluorescent MSP images, and using the area and dimension functions of Metamorph. For Fig. 3*C*, images of transitioning sperm cells were aligned using a MatLab algorithm. Briefly, for each image the center of mass of the sperm cell was calculated by detecting the cell contour with the Sobel method. Cell orientation was then defined by the smoothed tangent of the resulting trajectory. Images were superimposed via translation and rotation before making the kymograph. Membrane contours were observed by using the orthogonal planes function of Metamorph and taking the XZ section midway between the circle transcribed by the cell body and the tip of the lamellipodia at its longest. As a control, the XZ section bisecting the cell body was also taken. Using a Matlab script, the area and center of mass of the contour was calculated, an equivalent ellipse was generated, and the difference (both protrusions and invaginations) between the ellipse and the contour were measured. This area was divided by the total area of the contour to normalize for different sized cells and plotted in Fig. 4*C*. For Fig. 4*B*, contours were normalized to remove size differences and centered via their centers of mass. Filament orientations and lengths were quantified under different conditions by using images of sperm from *peel-1* promotor strains (EG5897) denoised using the program Safir (22) and analyzed manually in Metamorph. For length measurements, fibers were assumed to be straight. A bend or branch was taken to be the starting point of a new filament.

Tether Extrusion. Five to seven male worms were dissected into a drop of sperm media plus PVP and pronase (see above), and extruded sperm were allowed to activate for 3–5 min, then diluted 1:5 into sperm media plus 1:100 protease inhibitors (Sigma P8340), and 1–2 μL of Concanavalin A (Sigma) coated 2-μM beads (PolySciences) in a chamber made of a 1-cm diameter ring of clay sandwiched between two coverslips. Activated sperm cells were allowed to settle and adhere to the bottom coverslip. The optical trap setup (23) is based on a modified commercial Nikon Eclipse TE2000 inverted microscope with a nano LP100 piezo stage (Mad City Labs). Optical trapping was achieved in the infrared channel ($\lambda = 1{,}070$ nm) and bright field illumination in the near infrared channel ($750 < \lambda < 900$ nm). Concanavalin A-coated beads were held in the trap, adherent cells were moved to the bead using the piezo stage, and once adhered, slowly drawn away, pulling out a membrane tube. The force exerted by the tube was calculated from the equation $f = k(x - x_0)$, where f is force, k is the trap stiffness, and $x - x_0$ is the bead displacement, measured as described in ref. 24. For measuring tether force under hypoosmotic conditions, a tube was pulled in isotonic conditions and then water was flowed into the chamber, gradually lowering the osmotic strength of the medium. During the flow in, the tether force was recorded, while the tether was maintained at a constant length. The control was performed by maintaining a tube without injection of water.

ACKNOWLEDGMENTS. We warmly acknowledge Vincent Frasier and the PICT-IBiSA Imaging Facility at the Institut Curie for microscope use and support. We thank Cécile Sykes, Jean-François Joanny, Philippe Marcq, and Darius Köster for useful discussions and the *Caenorhabditis elegans* Genetics Center for worm strains. We thank Patricia Bassereau for the use of the laser tweezer setup. We thank Hannah S. Seidel and Leonid Kruglyak (Princeton University, Princeton, NJ) for the gift of the *peel-1* promotor, and Stefan Eimer (European Neuroscience Institute, Göttingen, Germany) for the gift of the *tagRFP-T* gene equipped with artificial introns. C.C. acknowledges Association pour la Recherche sur le Cancer for funding. This work and the salary of E.L.B. were funded by an Agence Nationale de la Recherche Jeune Chercheur grant and a Human Frontier Science Program Young Investigator grant (to J.P.).

1. Pollard TD, Borisy GG (2003) Cellular motility driven by assembly and disassembly of actin filaments. *Cell* 112:453–465.
2. Mogilner A, Oster G (1996) Cell motility driven by actin polymerization. *Biophys J* 71:3030–3045.
3. Raucher D, Sheetz MP (2000) Cell spreading and lamellipodial extension rate is regulated by membrane tension. *J Cell Biol* 148:127–136.
4. Sepsenwol S, Ris H, Roberts TM (1989) A unique cytoskeleton associated with crawling in the amoeboid sperm of the nematode *Ascaris suum*. *J Cell Biol* 108:55–66.
5. Nelson GA, Roberts TM, Ward S (1982) *Caenorhabditis elegans* spermatozoan locomotion: Amoeboid movement with almost no actin. *J Cell Biol* 92:121–131.
6. Sheetz MP, Dai J (1996) Modulation of membrane dynamics and cell motility by membrane tension. *Trends Cell Biol* 6:85–89.
7. Shaner NC, et al. (2008) Improving the photostability of bright monomeric orange and red fluorescent proteins. *Nat Methods* 5:545–551.
8. Seidel HS, et al. (2011) A novel sperm-delivered toxin causes late-stage embryo lethality and transmission ratio distortion in *C. elegans*. *PLoS Biol*, in press.
9. Frokjaer-Jensen C, et al. (2008) Single-copy insertion of transgenes in *Caenorhabditis elegans*. *Nat Genet* 40:1375–1383.
10. Ward S, Hogan E, Nelson GA (1983) The initiation of spermiogenesis in the nematode *Caenorhabditis elegans*. *Dev Biol* 98:70–79.
11. Bullock TL, Roberts TM, Stewart M (1996) 2.5 Å resolution crystal structure of the motile major sperm protein (MSP) of *Asaris suum*. *J Mol Biol* 263:284–296.
12. Dai J, Sheetz MP (1995) Mechanical properties of neuronal growth cone membranes studied by tether formation with laser optical tweezers. *Biophys J* 68:988–996.
13. Hochmuth RM, Shao J-Y, Dai J, Sheetz MP (1996) Deformation and flow of membrane into tethers extracted from neuronal growth cones. *Biophys J* 70:358–369.
14. Dai J, Sheetz MP (1999) Membrane tether formation from blebbing cells. *Biophys J* 77:3363–3370.
15. Waugh RE, Bauserman RG (1995) Physical measurements of bilayer-skeletal separation forces. *Ann Biomed Eng* 23:308–321.
16. Fedier A, Keller HU (1997) Suppression of bleb formation, locomotion, and polarity of Walker carcinosarcoma cells by hypertonic media correlates with cell volume reduction but not with changes in the F-actin content. *Cell Motil Cytoskeleton* 37:326–337.
17. Yoshida K, Soldati T (2006) Dissection of amoeboid movement into two mechanically distinct modes. *J Cell Sci* 119:3833–3844.
18. Renkawitz J, et al. (2009) Adaptive force transmission in amoeboid cell migration. *Nat Cell Biol* 11:1438–1443.
19. Liu AP, et al. (2008) Membrane-induced bundling of actin filaments. *Nat Phys* 4:789–793.
20. Strohmeier R, Bereiter-Hahn J (1987) Hydrostatic pressure in epidermal cells is dependent on Ca-mediated contractions. *J Cell Sci* 88:631–640.
21. Verkhovsky AB, et al. (2003) Orientational order of the lamellipodial actin network as demonstrated in living motile cells. *Mol Biol Cell* 14:4667–4675.
22. Boulanger J, et al. (2010) Patch-based nonlocal functional for denoising fluorescence microscopy image sequences. *IEEE Trans Med Imaging* 29:442–454.
23. Sorre B, et al. (2009) Curvature-driven lipid sorting needs proximity to demixing point and is aided by proteins. *Proc Natl Acad Sci USA* 106:5622–5626.
24. Neuman KC, Block SM (2004) Optical trapping. *Rev Sci Instrum* 75:2787–2809.